Bifunctional Bis-benzophenone as A Solid Additive for Non-fullerene Solar Cells

Pu Fan, Wenjian Sun, Xiaohua Zhang, Yao Wu, Qin Hu*, Qing Zhang*, Junsheng Yu*, Thomas P. Russell*

P. Fan, X.H. Zhang, Prof. J.S. Yu

State Key Laboratory of Electronic Thin Films and Integrated Devices

School of Optoelectronic Science and Engineering

University of Electronic Science and Technology of China (UESTC)

Chengdu 610054, P. R. China

E-mail: jsyu@uestc.edu.cn

P. Fan, Y. Wu, Dr. Q. Hu, Prof. T.P. Russell

Polymer Science and Engineering Department

University of Massachusetts Amherst

120 Governors Drive, Amherst, Massachusetts 01003, United States

E-mail: hihuqin@gmail.com, russell@mail.pse.umass.edu

Dr. Q. Hu, Prof. T.P. Russell

Materials Sciences Division, Lawrence Berkeley

National Laboratory, Berkeley, CA 94720, USA

E-mail: hihuqin@gmail.com, russell@mail.pse.umass.edu

W. Sun, Prof. Q. Zhang

Shanghai Key Laboratory of Electrical Insulation and Thermal Aging,

Department of Polymer Science and Engineering, School of Chemistry and

Chemical Engineering, Shanghai Jiaotong University,

Shanghai, 200240, P. R. China.

E-mail: qz14@sjtu.edu.cn

Keywords: solid additive, nonfullerene solar cell, thickness insensitivity, thermal stability

Abstract

Simultaneously improving efficiency and stability is critical for the commercial application of non-fullerene acceptor polymer solar cells (NFA-PSCs). Multifunctional solid additives have been considered as a potential route to tune the morphology of the active layer and optimize performance. In this work, photoinitiator bifunctional bis-benzophenone (BP-BP) is used as a solid additive, replacing solvent additives, in the PBDB-T:ITIC NFA system. With the addition of BP-BP, the intermolecular π-π stacking of PBDB-T and morphology is improved, leading to more balanced carrier transport and more effective exciton dissociation. Deices fabricated with BP-BP show a power conversion efficiency (PCE) of 11.89 %, with enhanced short-circuit current (J_{sc}) and fill factor (FF). Devices optimized with BP-BP show excellent reproducibility, insensitivity to thickness, and an improved thermal stability under atmospheric conditions without encapsulation. This work provides a new strategy for the application of solid additives in NFA-PSCs.

1. Introduction

Over the past few years, non-Fullerene acceptor (NFA) polymer solar cells (PSCs) have attracted significant attention, due to the marked increase in efficiencies.[1-5] Numerous strategies have been used to improve the power conversion efficiencies of NFA PSCs, including the synthesis of new materials,[6-8] morphology control of active layers,[9, 10] and the development of ternary and quaternary devices.[11, 12] PCEs of NFA-PSCs have recently exceeded 18%.[13, 14]Solvent additives have been widely used in NFA-PSCs to optimize the phase separation and domain size of the active layer without the introduction of extra processing steps. Common solvent additives employed in NFA-PSCs are 1,8-diiodooctane (DIO), diphenyl ether (DPE) and 1-chloronaphthalene (1-CN).[15-17] These high boiling point additives, due to their preferential affinity to one of the components, can effectively increase the ordering of the materials to improve the morphology and, hence, the PCE of NFA-PSC devices.[15]

However, after the fabrication of the active layer, these solvent additives cannot be fully removed in the thin film. When the devices are exposed to sunlight or high temperature, the residual additives can accelerate the degradation of organic materials and alter the morphology, negatively impacting device stability and reproducibility,[18, 19] and, consequently, the transfer of NFA-PSCs to application. Recently, Hou and coworkers designed several new volatile solid additives, and successfully used them to improve the PCE of NFA-PSCs.[20, 21] These additives not only improved intermolecular π-π stacking of the NFAs, but could also be removed with heating. Liu et al. used a nonvolatile solid additive, specifically chlorine-functionalized graphdiyne (GCl), to optimize the morphology of the active layer.[22] The nonvolatile property of GCI dramatically enhances the consistency in the morphology and performance of the active layer. These advances have led to

increased efforts in the use multifunctional solid additives in NFA-PSCs.[23, 24]

Except stability and reproducibility, in order to promote the commercial application of NF-PSCs, the appropriate processing thickness window is also a critical factor.[25, 26]For many common NFA systems, optimal performance can be achieved only when the thickness of active layer is ~100 nm.[27] Variations in the active layer thickness lead to variations in PCEs that can impact the roll-to-roll production of large scale, flexible devices.[28, 29] Consequently, developing active layers that are insensitive to thickness changes is important to the further development of NFA-PSCs.[29]

In this work, bifunctional bis-benzophenone (BP-BP), a photochemical crosslinking agent, is introduced into a typical NFA system, poly[(2,6-(4,8-bis(5-(2-ethylhexyl)thiophen-2-yl)- benzo[1,2-b:4,5-b']dithiophene))-alt-(5,5-(1',3'-di-2-thienyl-5',7'-bis(2-ethylhexyl)benzo[1',2'-c:4',5'-c']dithiophene-4,8-dione))]):3,9-bis(2-methylene-(3-(1,1-dicyanomethylene)-indanone))-5,5,11,11-tetrakis(4-hexylphenyl)-dithieno[2,3-d:2',3'-d']-s-indaceno[1,2-b:5,6-b']dithiophene) (PBDB-T:ITIC), as a solid additive. BP-BP does not volatilize and remains in the blend film, regulating the morphology and crystallinity. With the addition of 5wt % BP-BP, the PCE of the NFA-PSCs increased from 10.61 % to 11.89 %, with improved short-circuit current (J_{sc}) and fill factor (FF). The enhanced performance can be attributed to an optimized morphology, crystallinity, and balanced charge mobility with BP-BP. The BP-BP modified NFA-PSCs show a good thickness tolerance, reproducibility of device performance, and thermal stability, demonstrating a simple strategy to enhance the performance of NFA-PSCs.

2. Results and discussion

The molecular structures of BP-BP, PBDB-T, and ITIC are shown in **Figure 1**a. BP-BP has been

used as a UV-triggered photochemical crosslinking agent, especially with benzylic and tertiary hydrogen containing polymers (neither PBDB-T nor ITIC contain these two groups).[30-32] To confirm that crosslinking occurs between PBDB-T:ITIC and BP-BP, blend films were examined using Fourier transform infrared (FTIR) spectroscopy with 365 nm UV irradiation. As shown in Figure S1, after 5 min UV treatment for PBDB-T:ITIC:BP-BP, the transmission peak of PBDB-T:ITIC does not change. This indicates that crosslinking does not occur. In addition, the UV-treated PBDB-T:BP-BP film, as shown in Figure S2, can be removed with chlorobenzene washing, even with a BP-BP of 50wt %. Similar results were found for ITIC:BP-BP and PBDB-T:ITIC:BP-BP blend films. Consequently, BP-BP does not act as a crosslinker in these systems. Finally, to determine whether BP-BP will volatilize during the thermal annealing treatment of active layer, thermogravimetry analysis (TGA) was used and shown in Figure S3. It can be noted that the BP-BP begins to volatilize when the temperature exceeds 175 °C, indicating that BP-BP will remain in the active layer after annealing treatment of 100 °C. To further confirm this, profilometry and spectroscopic ellipsometry were used and the results are shown in Figure S4 and Figure S5, respectively.[21] Before annealing, The thickness of PBDB-T:ITIC and PBDB-T:ITIC:BP-BP blend films are similar (~109 nm). After thermal annealing at 100 °C 20 min, the thickness of the blend films with and without BP-BP doping showed no change. Even if the annealing temperature is increased to 120 °C, the thickness of BP-BP treated film still remains at ~109 nm. Spectroscopic ellipsometry also shows the same result. Under the condition that the incident angle and the wavelength of light are constant, the measured values of BP-BP treated film thickness at annealing temperatures of 0 °C, 100 °C and 120 °C are 108, 107.8 and 107.7 nm, respectively. These results show that BP-BP does not volatilize under the annealing conditions used in this work.

UV-vis absorption spectra of the pure and blended BP-BP and PBDB-T films were investigated. In

Figure 1 d, with BP-BP as an additive, the main absorption peak of PBDB-T sample showed a redshift of 5 nm, in comparison to the pure PBDB-T film, indicting an increased intermolecular π-π interaction of PBDB-T.[22] However, as shown in Figure S6, the absorption peaks of ITIC films with or without BP-BP showed no significant changes. The absorption spectra of PBDB-T:ITIC blend films (Figure S6) show that when BP-BP was added to the blend film, the PBDB-T absorption peak (633 nm) also redshirted, and the ITIC peak (700 nm) remained fixed. Consequently, only PBDB-T is influenced by the BP-BP.

For NFA-PSCs using an inverted device structure of ITO/ZnO/PBDB-T:ITIC (with and without BP-BP)/MoOx/Ag (Figure 1e), the current density-voltage (*J-V*) curves and device parameters were obtained and are shown in **Figure 2**a and Table 1. The control device with active layer of PBDB-T:ITIC yielded an average PCE of 10.61 %, with an open-circuit voltage (V_{oc}) of 0.872 V, a J_{sc} of 18.45 mA cm^{-2}, and a FF of 65.98 %. After doping with 5wt % BP-BP, the average PCE NFA-PSCs increased significantly to 11.89 %, due to an increased J_{sc} and FF (19.31 mA cm^{-2} and 70.28 %, respectively). However, increasing the concentration of BP-BP to 10wt %, the PCE decreased to 10.83 %, with a reduced J_{sc} and FF (Figure S7 and Table S1), indicating there is an optimal concentration of BP-BP. Furthermore, the PCE of devices with and without BP-BP did not change significantly after exposure to 365 nm UV radiation (Figure S8), indicating that the crosslinking with BP-BP, if it occurred, did not influence the performance of PBDB-T:ITIC:BP-BP NFA-PSCs.

The external quantum efficiencies (EQE) of NFA-PSCs were determined and are shown in Figure S9. The devices processed without BP-BP had an integrated current density of 18.42 mA cm^{-2}, while with BP-BP a value of 19.27 mA cm^{-2} was found, matching well with the J_{sc} values in the *J-V* measurements. Figure S10 shows the distribution of PCEs obtained for 16 devices with and without

BP-BP. In comparison to the control devices, the PCE distribution of NFA-PSCs processed with BP-BP narrowed significantly, suggesting a better reproducibility of devices.

We characterized the carrier dynamics to understand the origins of the improvement in device performance. To probe the effect of BP-BP on charge collection and exciton dissociation in NFA-PSCs, the net photocurrent density (J_{ph}) was measured as a function of the effective voltage (V_{eff}) and shown in Figure S11. J_{ph} is defined as J_L-J_D, where J_L and J_D are the photocurrent density and dark current density, respectively. V_{eff} could be calculated usingV_0-V, where V_0 is the voltage when J_{ph}=0 and V is the applied bias voltage.[33]The saturation current (J_{sat}) of the control device is 19.02 mA cm^{-2}, and for devices with BP-BP J_{sat} =19.63 mA cm^{-2}. The charge dissociation efficiency (P) of NFA-PSCs was estimated as P=J_{sc}/J_{sat}.[34] With BP-BP, P increased from 97 % to 98.4 %, indicating that exciton dissociation became more efficient.

Bimolecular recombination plays an important role in NFA-PSCs. The dependence of J_{sc}on light intensity (P_{light}) was measured. In general, $J_{sc} \propto P_{light}^{\alpha}$, where the exponent α is related to the degree of recombination. When α ~ 1, bimolecular recombination is low.[35] As shown in Figure 2b, the values of α for NFA-PSCs with and without BP-BP are 0.989 and 0.974, respectively meaning that, in comparison to the control devices, BP-BP suppress bimolecular recombination in PBDB-T:ITIC more effectively.

To probe trap-assisted recombination in the devices, the slope of V_{oc} as a function of ln(P_{light}) was determined and shown in Figure 2c. If bimolecular recombination is dominant, the slope should be close to 1 K_BT/q (where K_B is Boltzmann's constant, T is the absolute temperature, and q is the elementary charge), and a slope close to 2 K_BT/q indicates that trap-assisted recombination is

dominant.[29] Control devices without BP-BP show a slope of 1.28 K_BT/q, while the devices using BP-BP show a lower slope of 1.19 K_BT/q, indicating that the trap-assisted recombination in the active layer is suppressed with the addition of BP-BP, which could lead to increased FF.

To determine the influence of BP-BP addition on the charge mobility, the space charge limited current (SCLC) method was used and the results are shown in Figure 2d. For hole-only devices, a device structure of ITO/PEDOT:PSS (40 nm)/active layer (110 nm)/MoOx (10 nm)/Ag was used, and for electron-only devices the architecture was ITO/ZnO (30 nm)/active layer (110 nm)/Bphen (8 nm)/Ag. The corresponding hole and electron mobilities are shown in Table 2. With BP-BP, the hole mobility of NFA-PSCs increased from 1.96×10^{-4} to 2.15×10^{-4} cm^2 V^{-1} s^{-1}, and the electron mobility showed a dramatic increase from 1.06×10^{-4} to 2.47×10^{-4} cm^2 V^{-1} s^{-1}. Consequently, the addition of BP-BP improved both the charge mobilities, especially the electron mobility. The hole and electron mobilities became more balanced with the addition of BP-BP, in agreement with the improved J_{sc} and FF of the NFA-PSCs[36, 37]. Due to the insulating nature of BP-BP, the enhanced charge mobility can be attributed to the improved morphology and increased crystallinity of the active layer.[32]

Atomic force microscopy (AFM) was carried out to study the surface characteristics of the active layers. As shown in **Figure 3**a-b, similar surface morphologies are observed for PBDB-T:ITIC films without or with BP-BP doping. The corresponding root-mean-square (RMS) surface roughnesses are 4.9 and 4.1 nm, respectively. This suggests that the proper amount of BP-BP as solid additive will not significantly affect the surface morphology of active layer. The phase characteristics of the surfaces of different active layers are also similar, as shown in Figure 3e-f. No obvious differences were seen by transmission electron microscopy (TEM) measurements (as shown in Figure S12) of the active layer with and without BP-BP doping.

Grazing-incidence wide-angle X-ray scattering (GIWAXS) was used to assess the influence of BP-BP on the ordering. The 2D GIWAXS profiles and the corresponding integrated line profiles are shown in **Figure 4**. BP-BP did not influence the in-plane (IP) scattering of PBDB-T (Figure 4a-c). However, in the out-of-plane (OOP) direction, the PBDB-T:BP-BP blend showed a stronger (010) peak at 1.71 $Å^{-1}$, indicating that the π-π stacking of PBDB-T can be enhanced by the BP-BP.[38, 39] The corresponding crystal coherence length (CCL) was calculated using a Scherrer analysis of the full width at half maximum (FWHM). The CCL of the (010) peak for PBDB-T is 1.8 nm, which increased to 2.0 nm for the PBDB-T:BP-BP film. In Figure 4d-f, the diffraction peaks of the pure ITIC and ITIC:BP-BP films in the IP and OOP directions are similar, the (100) peak in IP direction of pure ITIC and ITIC:BP-BP are located at 0.29 $Å^{-1}$, and the (010) peak in OOP direction are all at 1.71 $Å^{-1}$, indicating that the introduction of BP-BP did not change the molecular order of ITIC. For the PBDB-T:ITIC blend films in Figure 4g-i, a stronger (010) peak in the OOP direction was evident, and the corresponding CCLs of PBDB-T:ITIC blend films without and with BP-BP are 1.6 and 1.8 nm, respectively. Along with the absorption spectra, it can be concluded that BP-BP enhances the π-π stacking of PBDB-T in the blend film, with a face-on orientation, that is beneficial to the charge transport.

The thickness of the active layer was fixed at ~110 nm in the studies discussed above. To realize large-scale production of NFA-PSCs, a wide processing window in active layer thickness is necessary. The thickness of the active layer was changed, while fixing the mass ratio of PBDB-T, ITIC, and BP-BP. As shown in Table 1, after increasing the thickness of active layer from 110 to 230 nm, the V_{oc} of all devices did not decrease significantly, but the J_{sc} and FF showed an obvious thickness-dependence. For the control device, when the thickness of active layer increases to 230 nm, the J_{sc} increases from 18.45 to 19.22 mA cm^{-2}, and the FF decreased from 65.98 to 58.33 %. For the devices with BP-BP, the

J_{sc} increased from 19.31 to 20.10 mA cm^{-2}, and the FF decreased from 70.28 to 66.03 %. When the thickness of PBDB-T:ITIC was increased to 230 nm, the PCE shows a marked decline, indicating that the performance of the PBDB-T:ITIC system is sensitive to active layer thickness. In comparison to the control devices, the devices with BP-BP maintained 97 % of original PCE after increasing the thickness by a factor of two, indicating a thickness-tolerance of the PBDB-T:ITIC:BP-BP active layer from 110 to 230 nm.

Theoretically, as the thickness of active layer increases, more photons are absorbed, which leads to the improvement of J_{sc}. However, the morphology can also be affected by the thickness change with more trap-assisted recombinations within the active layer that lead to a decrease of FF.[27] As shown in Figure 3c-d, in comparison to a PBDB-T:ITIC film of 110 nm, the morphology of the 230 nm film shows a significant change, including an increase in the RMS roughness (from 4.9 to 12.6 nm), as evidenced in the topography (3D AFM images are shown in Figure S13). The increased roughness and larger film topography are adverse to charge extraction and dissociation properties of NFA-PSCs, causing a decreased PCE. However, with BP-BP, the RMS roughness of a 230 nm film is 8.8 nm, much lower than that of the control film, and a change of film topography is not obvious. The corresponding phase images also show a similar trend (Figure 3g-h). Consequently, with BP-BP the surface roughness remains low while, as shown in Figure S14 in the GIWAXS, the intermolecular π-π stacking of PBDB-T in 230 nm blend is stronger. Therefore, the PBDB-T:ITIC:BP-BP based NFA-PSCs show excellent thickness-insensitivity due to the optimization of the morphology.

Finally, the effect of thermal treatment on the PCE of unencapsulated NFA-PSCs was investigated by cycling the devices between 80 °C and 140 °C[40, 41] in air at a 40-60 % humidity level. The corresponding normalized PCE is shown in **Figure 5**. After heating to 80 °C for 168 hours, the

control devices retained 64 % of their original PCE. With BP-BP, the devices retained 86 % of their original value. This indicates that the thermal stability of PBDB-T:ITIC is improved with the addition of BP-BP. Similar behavior is seen at 140 °C (Figure 5b). At 140 °C, compared to the control devices, the PCE of BP-BP-containing devices retained a higher percentage of their original values after 60 min. Consequently, BP-BP has markedly enhanced the thermal stability of the devices.

To compare the performance and stability of the NFA-PSCs prepared using the common solvent additive DIO or solid additive BP-BP, a series of PBDB-T:ITIC based devices were fabricated with 0.5 % DIO to investigate the differences in performance with 5 % BP-BP doping. As shown in Figure S15a and Table S2, the PCE of devices using DIO (11.65 %) is similar to those based on BP-BP, and the DIO treated devices show higher J_{sc} (19.58 mA cm^{-2}) and lower FF (67.62 %). Consequently, both DIO and BP-BP significantly enhance the PCE of the PBDB-T:ITIC based NFA-PSCs. However, when comparing the range of PCEs (Figure S15b), The reproducibility of the devices based on BP-BP is better than those based using DIO. From the thermal stability test in Figure S15c, it can be seen that after 168 hours of aging at 80 °C for 168 hours with DIO as an additive, the PCE of the device is only 58% of the initial value, which is significantly lower than that of the device using BP-BP. Consequently, the solid additive BP-BP is better than DIO for reproducibility and thermal stability of the NFA-PSCs.

The thickness dependence of the DIO treated devices was also studied. As shown in Table S2, after increasing the thickness of active layer from 110 nm to 230 nm, the PCE of DIO treated devices decreases to 10.87 %. From the AFM images (Figure S16), we can see that the surface morphology of DIO treated active layer is very similar to that of undoped active layer, which suggests that BP-BP can regulate the morphology of thick films more effectively than DIO. These results show that BP-BP has more potential as an additive to promote the commercial application of PSCs.

Conclusion

The photoinitiator bifunctional bis-benzophenone (BP-BP) had been successfully used as a solid additive in PBDB-T:ITIC NFA-PSCs. The red-shift of absorption peak and the change in the GIWAXS indicate that the introduction of BP-BP modifies the intermolecular ordering of PBDB-T and enhances the π-π stacking. The results of corresponding electrical measurements show that BP-BP can not only balance the charge mobility of electrons and holes in the active layer, but also improve the charge collection ability and suppress the trap-assisted recombination. As a result, both the Jsc and FF show a dramatic improvement, the PCE is increased from 10.61 to 11.89 % after the addition of BP-BP. In comparison to control devices, the BP-BP modified devices show a better reproducibility, a thickness-insensitivity, and a thermal stability in the air. Our work presents a new strategy for developing NFA-PSCs towards further commercial application.

Supporting Information

Supporting Information is available from the Wiley Online Library or from the author.

Acknowledgments

This work was supported by the National Key R&D Program of China (Grant No. 2018YFB0407102), the Foundation of National Natural Science Foundation of China (NSFC) (Grant Nos. 61421002, 61675041, 21674060 & 51703019), the Project of Science and Technology of Sichuan Province (Grant Nos. 2019YFG0121, 2019YJ0178, 2020YFG0279 & 2020YFG0281). Y.W., Q.H. and T.P.R. were supported by the Office of Naval Research, under Contract N00014-17-1-2241. This work is also sponsored by Sichuan Province Key Laboratory of Display Science and Technology. P. Fan gratefully acknowledges the Chinese Scholarship Council (No. 201806070051) for partial support of this work.

Received: ((will be filled in by the editorial staff))
Revised: ((will be filled in by the editorial staff))
Published online: ((will be filled in by the editorial staff))

References

[1] P. Cheng, G. Li, X. Zhan, Y. Yang, *Nat. Photonics* **2018**, 12, 131.

[2] G. Zhang, J. Zhao, P. C. Y. Chow, K. Jiang, J. Zhang, Z. Zhu, J. Zhang, F. Huang, H. Yan, *Chem. Rev.* **2018**, 118, 3447.

[3] C. Yan, S. Barlow, Z. Wang, H. Yan, A. K. Y. Jen, S. R. Marder, X. Zhan, *Nat. Rev. Mater.* **2018**, 3, 18003.

[4] J. Hou, O. Inganas, R. H. Friend, F. Gao, *Nat. Mater.* **2018**, 17, 119.

[5] K. Gao, Y. Kan, X. Chen, F. Liu, B. Kan, L. Nian, X. Wan, Y. Chen, X. Peng, T. P. Russell, Y. Cao, A. K. Jen, *Adv. Mater.* **2020**, 32, 1906129.

[6] S. Li, L. Zhan, Y. Jin, G. Zhou, T. K. Lau, R. Qin, M. Shi, C. Z. Li, H. Zhu, X. Lu, F. Zhang, H. Chen, *Adv. Mater.* **2020**, 32, 2001160.

[7] Z. Hu, J. Wang, X. Ma, J. Gao, C. Xu, K. Yang, Z. Wang, J. Zhang, F. Zhang, *Nano Energy* **2020**, 78, 105376.

[8] H. Yao, F. Bai, H. Hu, L. Arunagiri, J. Zhang, Y. Chen, H. Yu, S. Chen, T. Liu, J. Y. L. Lai, Y. Zou, H. Ade, H. Yan, *ACS Energy Lett.* **2019**, 4, 417.

[9] L. Zhu, M. Zhang, G. Zhou, T. Hao, J. Xu, J. Wang, C. Qiu, N. Prine, J. Ali, W. Feng, X. Gu, Z. Ma, Z. Tang, H. Zhu, L. Ying, Y. Zhang, F. Liu, *Adv. Energy Mater.* **2020**, 10, 1904234.

[10] D. Liu, K. Zhang, Y. Zhong, C. Gu, Y. Li, R. Yang, *J. Mate. Chem. A* **2018**, 6, 18125.

[11] Q. An, J. Wang, W. Gao, X. Ma, Z. Hu, J. Gao, C. Xu, M. Hao, X. Zhang, C. Yang, F. Zhang, *Sci. Bull.* **2020**, 65, 538.

[12] J. Gao, J. Wang, Q. An, X. Ma, Z. Hu, C. Xu, X. Zhang, F. Zhang, *Sci. China Chem.* **2019**, 63, 83.

[13] Q. Liu, Y. Jiang, K. Jin, J. Qin, J. Xu, W. Li, J. Xiong, J. Liu, Z. Xiao, K. Sun, S. Yang, X. Zhang, L. Ding, *Sci. Bull.* **2020**, 65, 272.

[14] Y. Cui, H. Yao, J. Zhang, K. Xian, T. Zhang, L. Hong, Y. Wang, Y. Xu, K. Ma, C. An, C. He, Z. Wei, F. Gao, J. Hou, *Adv. Mater.* **2020**, 32, 1908205.

[15] J. Sun, Z. Zhang, X. Yin, J. Zhou, L. Yang, R. Geng, F. Zhang, R. Zhu, J. Yu, W. Tang, *J. Mate. Chem. A* **2018**, 6, 2549.

[16] D. He, F. Zhao, J. Xin, J. J. Rech, Z. Wei, W. Ma, W. You, B. Li, L. Jiang, Y. Li, C. Wang, *Adv. Energy Mater*. **2018**, 8, 1802050.

[17] Q. Wu, D. Zhao, J. Yang, V. Sharapov, Z. Cai, L. Li, N. Zhang, A. Neshchadin, W. Chen, L. Yu, *Chem. Mater.* **2017**, 29, 1127.

[18] C. McDowell, M. Abdelsamie, M. F. Toney, G. C. Bazan, *Adv. Mater.* **2018**, 30, 1707114.

[19] B.J. Tremolet de Villers, K.A. O'Hara, D.P. Ostrowski, P.H. Biddle, S.E. Shaheen, M.L. Chabinyc, D.C. Olson, N. Kopidakis, *Chem. Mater.* **2016**, 28, 876.

[20] R. Yu, H. Yao, Z. Chen, J. Xin, L. Hong, Y. Xu, Y. Zu, W. Ma, J. Hou, *Adv. Mater.* **2019**, 31, 1900477.

[21] R. Yu, H. Yao, L. Hong, Y. Qin, J. Zhu, Y. Cui, S. Li, J. Hou, *Nat. Commun.* **2018**, 9, 4645.

[22] L. Liu, Y. Kan, K. Gao, J. Wang, M. Zhao, H. Chen, C. Zhao, T. Jiu, A. K. Jen, Y. Li, *Adv. Mater.* **2020**, 32, 1907604.

[23] J. Cai, H. Wang, X. Zhang, W. Li, D. Li, Y. Mao, B. Du, M. Chen, Y. Zhuang, D. Liu, H.-L. Qin, Y. Zhao, J. A. Smith, R. C. Kilbride, A.J. Parnell, R.A. L. Jones, D.G. Lidzey, T. Wang, *J. Mate. Chem. A* **2020**, 8, 4230.

[24] X. Du, X. Li, H. Lin, L. Zhou, C. Zheng, S. Tao, *J. Mate. Chem. A* **2019**, 7, 7437.

[25] J.L. Wang, K.K. Liu, L. Hong, G.Y. Ge, C. Zhang, J. Hou, *ACS Energy Lett.* **2018**, 3, 2967.

[26] B. Guo, W. Li, X. Guo, X. Meng, W. Ma, M. Zhang, Y. Li, *Adv. Mater.* **2017**, 29, 1702291.

[27] W. Gao, Q. An, M. Hao, R. Sun, J. Yuan, F. Zhang, W. Ma, J. Min, C. Yang, *Adv. Funct. Mater.* **2020**, 30, 1908336.

[28] Z. Wang, H. Jiang, X. Liu, J. Liang, L. Zhang, L. Qing, Q. Wang, W. Zhang, Y. Cao, J. Chen, *J. Mate. Chem. A* **2020**, 8, 7765.

[29] T. Zhang, G. Zeng, F. Ye, X. Zhao, X. Yang, *Adv. Energy Mater.* **2018**, 8, 1801387.

[30] N. D. Carbone, M. Ene, J. R. Lancaster, J. T. Koberstein, *Macromolecules* **2013**, 46, 5434.

[31] G. T. Carroll, L. Devon Triplett, A. Moscatelli, J. T. Koberstein, N. J. Turro, *J. Appl. Polym. Sci.* **2011**, 122, 168.

[32] Y. Zou, Y. Liu, M. Ban, Q. Huang, T. Sun, Q. Zhang, T. Song, B. Sun, *Nanoscale Horiz.* **2017**, 2, 156.

[33] S. Dai, T. Li, W. Wang, Y. Xiao, T. K. Lau, Z. Li, K. Liu, X. Lu, X. Zhan, *Adv. Mater.* **2018**, 30, 1706571.

[34] L. Nian, Y. Kan, H. Wang, K. Gao, B. Xu, Q. Rong, R. Wang, J. Wang, F. Liu, J. Chen, G. Zhou, T. P. Russell, A. K. Y. Jen, *Energy Environ. Sci.* **2018**, 11, 3392.

[35] Y. Wu, H. Bai, Z. Wang, P. Cheng, S. Zhu, Y. Wang, W. Ma, X. Zhan, *Energy Environ. Sci.* **2015**, 8, 3215.

[36] C. Xu, H. Chen, Z. Zhao, J. Gao, X. Ma, S. Lu, X. Zhang, Z. Xiao, F. Zhang, J. Energy Chei. **2020**.

[37] Q. An, J. Wang, X. Ma, J. Gao, Z. Hu, B. Liu, H. Sun, X. Guo, X. Zhang, F. Zhang, *Energy Environ. Sci.* **2020**.

[38] Q. Hu, W. Chen, W. Yang, Y. Li, Y. Zhou, B. W. Larson, J. C. Johnson, Y.H. Lu, W. Zhong, J. Xu, L. Klivansky, C. Wang, M. Salmeron, A. B. Djurišić, F. Liu, Z. He, R. Zhu, T. P. Russell, *Joule* **2020**, 4, 1575.

[39] Y. Zheng, J. Huang, G. Wang, J. Kong, D. Huang, M. Mohadjer Beromi, N. Hazari, A. D. Taylor, J. Yu, *Mater. Today* **2018**, 21, 79.

[40] H. Hu, L. Ye, M. Ghasemi, N. Balar, J. J. Rech, S. J. Stuard, W. You, B. T. O'Connor, H. Ade, *Adv. Mater.* **2019**, 31, 1808279.

[41] W. Yang, Z. Luo, R. Sun, J. Guo, T. Wang, Y. Wu, W. Wang, J. Guo, Q. Wu, M. Shi, H. Li, C. Yang, J. Min, *Nat. Commun.* **2020**, 11, 1218.

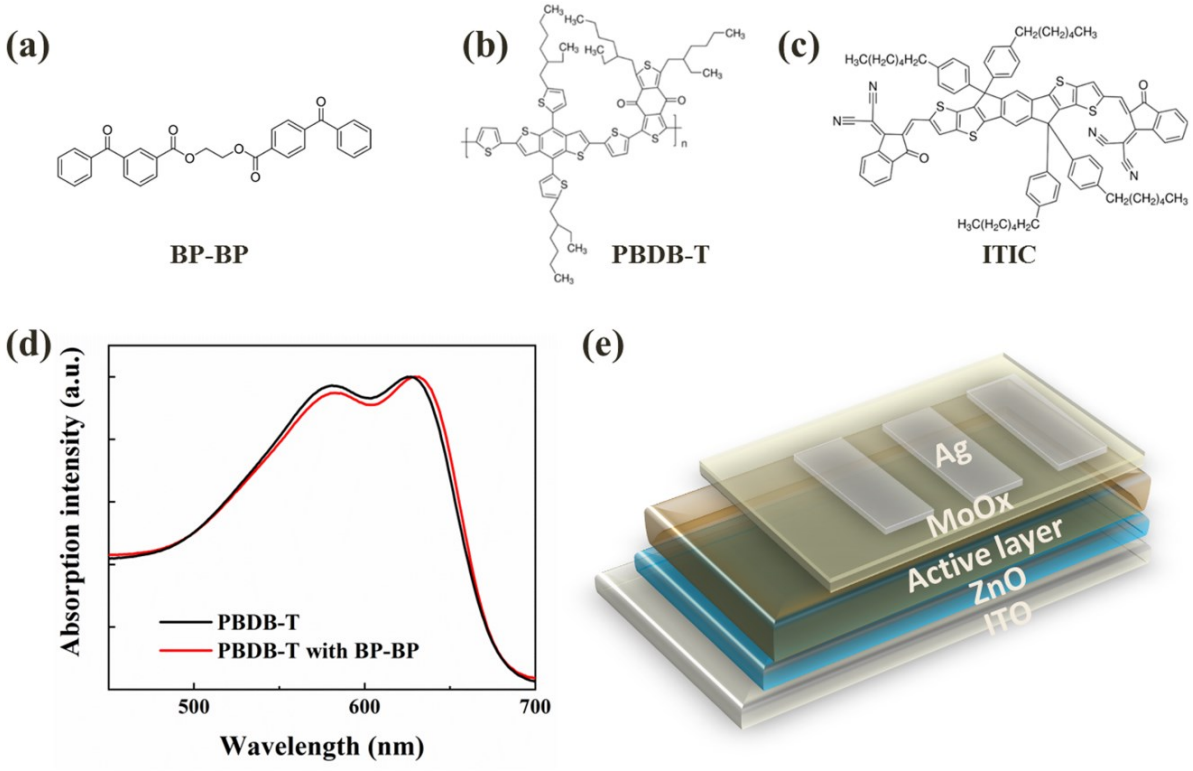

Figure 1. Chemical structures of (a) BP-BP, (b) PBDB-T (c) and ITIC; (d) UV–vis absorption spectra of PBDB-T with and without BP-BP; (e) inverted device structure of NFA-PSCs in this work.

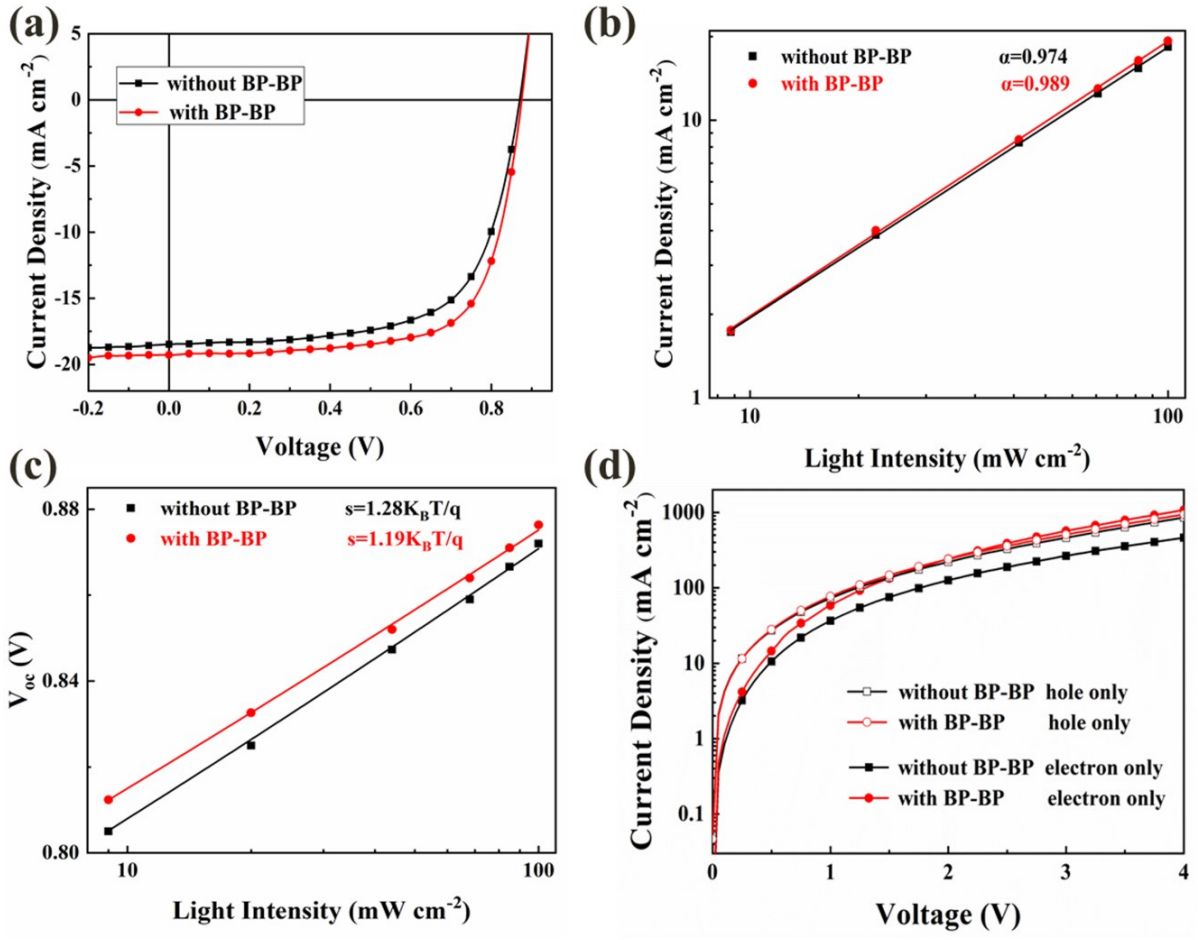

Figure 2. (a) *J-V* characteristics of PBDB-T:ITIC NFA-PSCs with and without BP-BP solid additive; light intensity dependence of (b) J_{sc} and (c) V_{oc} of NFA-PSCs with and without BP-BP; (d) hole and electron only mobility of devices by SCLC method.

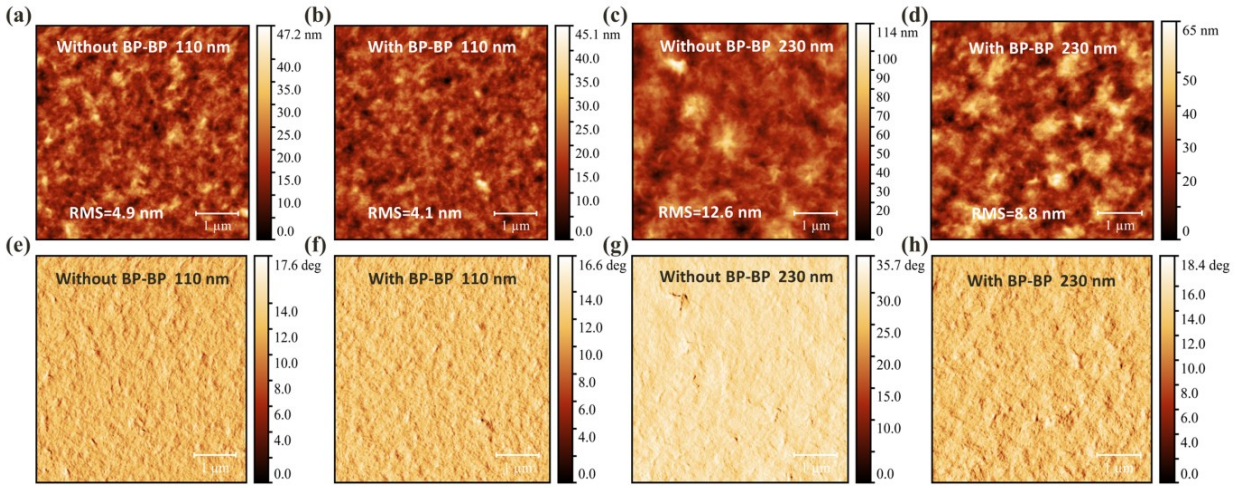

Figure 3. (a-d) AFM images and (e-h) phase images of PBDB-T:ITIC active layers with and without BP-BP under the condition of different thickness.

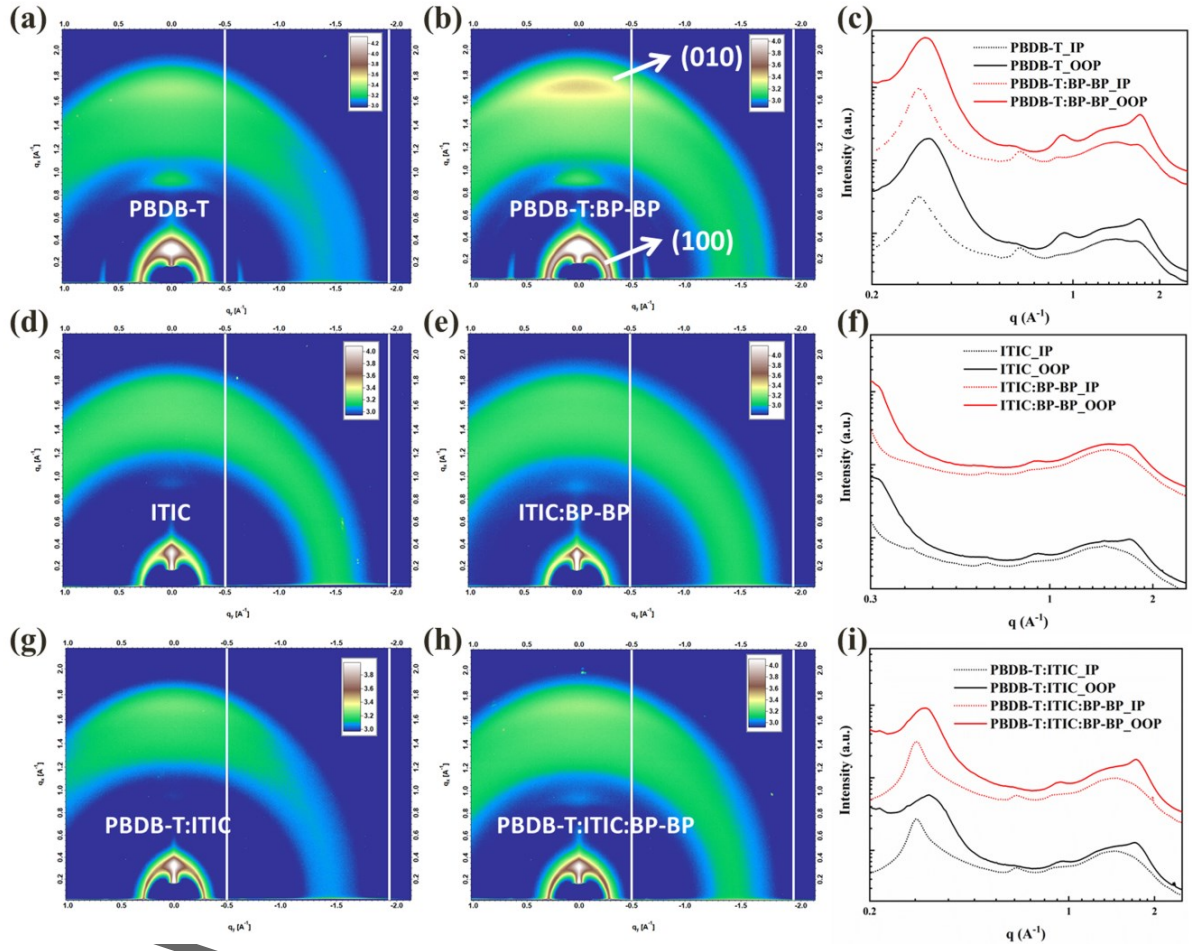

Figure 4. 2D GIWAXS patterns and profiles of films based on (a-c) PBDB-T, (d-f) ITIC, and (g-i) PBDB-T:ITIC processed with and without BP-BP doping.

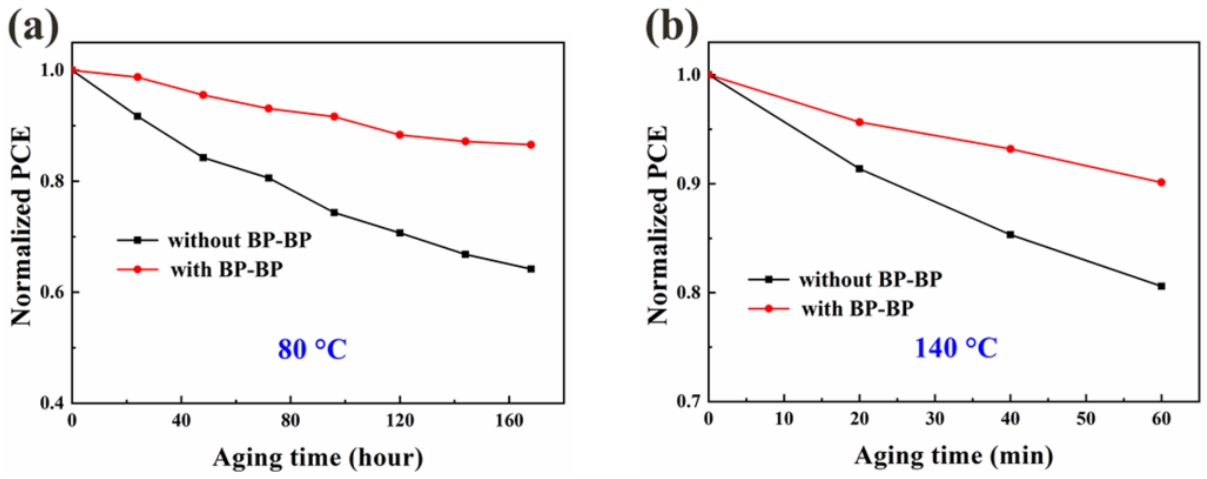

Figure 5. Thermal stability of unencapsulated NFA-PSCs with and without BP-BP stored in the atmosphere at (a) 80 °C and (b) 140 °C

Table 1. Key photovoltaic parameters of PBDB-T:ITIC NFA-PSCs with different BP-BP doping concentrations and thickness [a]

BP-BP (wt %)	Thickness of active layer (nm)	V_{OC} (V)	J_{sc} (mA cm^{-2})	calculated J_{sc} (mA cm^{-2})	FF (%)	PCE (%)[b]
0	110	0.872	18.45	18.42	65.98	10.61±0.32 (11.17)
5	110	0.877	19.31	19.27	70.28	11.89±0.17 (12.14)
0	230	0.865	19.22	-	58.33	9.69±0.45 (10.27)
5	230	0.873	20.10	-	66.03	11.57±0.20 (11.82)

[a]All parameters are average value collected from 16 devices.

[b]The best PCE is in brackets.

Table 2. Charge mobility of NFA-PSCs with or without BP-BP

BP-BP (wt %)	Hole mobility μ_h (cm^2 V^{-1} s^{-1})	Electron mobility μ_e (cm^2 V^{-1} s^{-1})	μ_h/μ_e
0	1.96×10^{-4}	1.06×10^{-4}	1.85
5	2.15×10^{-4}	2.47×10^{-4}	0.88

Table of Contents:

The photoinitiator bifunctional bis-benzophenone had been introduced into non-fullerene solar cells as a multifunctional solid additive for the first time. The doping of this solid additive could not only modify the polymer order and firm morphology of active layer to improve device performance, but also achieve better reproducibility, thickness insensitivity, and thermal stability for the non-fullerene solar cells.

Keywords: solid additive, nonfullerene solar cell, thickness insensitivity, thermal stability

Pu Fan, Wenjian Sun, Xiaohua Zhang, Yao Wu, Qin Hu, Qing Zhang*, Junsheng Yu*, Thomas P. Russell**

Bifunctional Bis-benzophenone as A Solid Additive for Non-fullerene Solar Cells